Effective surface Debye temperature for NiMnSb.100. epitaxial films

C.N. Borca
University of Nebraska-Lincoln

Takashi Komesu
University of Nebraska-Lincoln, tkomesu2@unl.edu

Hae-kyung Jeong
University of Nebraska-Lincoln, hjeong@unl.edu

Peter A. Dowben
University of Nebraska-Lincoln, pdowben@unl.edu

D. Ristoiu
Laboratoire L. Ne´el, CNRS, BP 166 X, 38042 Grenoble Cedex 9, France

See next page for additional authors

Authors

C.N. Borca, Takashi Komesu, Hae-kyung Jeong, Peter A. Dowben, D. Ristoiu, Ch. Hordequin, J. Pierre, and J. P. Nozie`res

Effective surface Debye temperature for NiMnSb(100) epitaxial films

C. N. Borca, Takashi Komesu, Hae-kyung Jeong, and P. A. Dowben[a)]
Department of Physics and Astronomy and the Center for Materials Research and Analysis,
Behlen Laboratory, University of Nebraska, Lincoln, Nebraska 68588-0111

D. Ristoiu, Ch. Hordequin, J. Pierre, and J. P. Nozières
Laboratoire L. Néel, CNRS, BP 166 X, 38042 Grenoble Cedex 9, France

The surface Debye temperature of the NiMnSb (100) epitaxial films has been obtained using low energy electron diffraction, inverse photoemission, and core-level photoemission. The normal dynamic motion of the (100) surface results in a value for the effective surface Debye temperature of 145 ± 13 K. This is far smaller than the bulk Debye temperature of 312 ± 5 K obtained from wave vector dependent inelastic neutron scattering. The large difference between these measures of surface and bulk dynamic motion indicates a soft and compositionally different (100) surface. © *2000 American Institute of Physics.* [S0003-6951(00)05127-5]

Interest in NiMnSb Heusler alloys remains active because of the relatively high Curie temperature ($\sim$730 K) and like all half metallic systems has potential technological applications in spin polarized electron transport devices.[1] In spin tunnel junction devices, the interfaces play an important role in the value of the tunneling magnetoresistance (TMR). The interface should have, ideally, 100% polarization at the Fermi energy and well characterized ''matched'' Fermi crossings. Unfortunately, the polarization of NiMnSb is very sensitive to composition and defects[2,3] and the NiMnSb(100) surface is observed to be very fragile.[2,4] The thermal motions of the surface atoms dictates many of the physical and chemical properties of a surface, such as surface diffusion,[5] anharmonicity leading to roughening transitions,[6] surface reconstructions,[7] and influence the extent of composition inhomogenities, including defects. The key descriptive parameter of the dynamic motions of atoms on the surface, as well as in the bulk, is the Debye temperature.

In this letter we investigate the effective surface Debye temperature of the NiMnSb(100) which we compare to the bulk Debye temperature calculated from the phonon dispersion curves obtained from inelastic neutron scattering. This comparison is one of only a limited number of such studies in complex compound materials[8,9] and the first for the Heusler alloys.

The bulk Debye temperature of single crystals can be estimated from application of the Debye model and the phonon dispersion curves.[10] In this model, the upper limit v_D to the frequency is to be obtained from the normalizing condition that the total number of oscillatory modes is equal to $3rN_A$ per mole, where r is the number of atoms per unit cell (and N_A is Avogadro's number). The quantity v_D is with the related parameter θ_D by

$$v_D = \frac{k_B}{h} \theta_D, \tag{1}$$

where h is Planck's constant and k_B is Boltzman's constant. Thus, the frequency limit $_D$ and the related parameter θ_D, the Debye temperature, can be obtained from the formula[10]

$$\frac{4\pi V}{3}(c_L^{-3} + 2c_T^{-3})v_D^3 = 3rN_A, \tag{2}$$

in which V is the molar volume and c_L, c_T are the corresponding longitudinal and transversal wave velocity. For cubic crystals, the velocities are related to the elastic constants C_{11}, C_{44}, and C_{12} along the main axis of symmetry (100), (110), and (111), as described in Ref. 11. For values of the scattering vector q close to zero, the dispersion of the acoustic oscillatory modes is linear, and the slope of this linear dependence is related to particular elastic constants, depending on the scanning direction.

The effective surface Debye temperature of single crystal materials can be investigated by low energy electron diffraction (LEED),[12–14] x-ray photoemission spectroscopy (XPS), or valence band photoemission (PES),[15] inverse photoemission[16] as well as atom beam scattering and other surface sensitive techniques (Ref. 15 and the references therein). Generally, in electron scattering and electron spectroscopy techniques it is assumed, in the absence of a surface phase transition, that the emerging electron beam intensity depends exponentially on the sample temperature[13,14]

$$I = I_0 \exp(-2W) \tag{3}$$

$$2W = \frac{3\hbar^2 T(\Delta k)^2}{2mk_B\theta_D^2}, \tag{4}$$

where W is the Debye–Waller factor, $\hbar$ is Planck constant, T is the sample temperature, $\hbar(\Delta k)$ is the electron momentum transfer, m is the mass of the scattering center, k_B is the Boltzmann constant, and θ_D is the effective surface Debye temperature. This surface θ_D is dominated by the dynamic motions normal to the surface in almost all experiments and typically does not contain significant in-plane or anharmonic contributions to the true surface Debye temperature,[15] and therefore tends to be independent of surface orientation. [The major exception is high-resolution electron energy loss spectroscopy of the surface (where the details of phonon dispersion can matter) and, in off-specular scattering geometries, nondipole active modes can be probed].

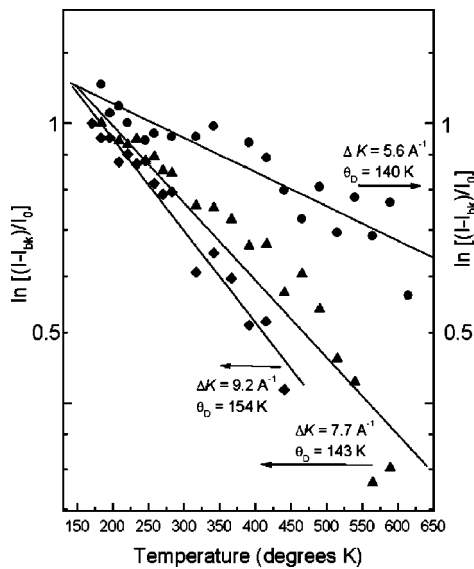
[a)]Electronic mail: pdowben@unl.edu

FIG. 1. Logarithm of the intensities of the diffracted electron spots obtained in LEED, after background (I_{bk}) subtraction and normalization to the value (I_0) at the lowest temperature. The three sets of data were obtained using different incident electron energies: 33 (circles), 58 (up triangle), and 83 eV (diamond).

To apply Eqs. (3) and (4) to LEED or photoemission, we need to consider the geometry of the experiment and the mass of the scattering centers. For LEED, we have used diffracted electron beams with the scattering vector (Δk) close to the normal to the surface (leading to the dominant role of normal lattice vibrations). The mass of the scattering centers is an average of the three different atomic masses contained in a unit cell with the scattering vector being calculated from

$$\Delta k = 2k \cos \frac{\theta}{2} = \frac{4\pi}{\lambda} \cos \frac{\theta}{2}, \quad (5)$$

where θ is the angle between the incoming and outgoing electron beams and λ is the wavelength of the electrons.

In the case of photoemission spectroscopy (XPS and PES) ($\theta = 0$), the momentum transfer is equal to the momentum of the emitted electron: $\Delta k = 2\pi/\lambda$. In our experiments, we monitored the photoelectron intensity from the $3d$ shell of the Sb atoms (using Mg$K\alpha$ radiation) and appropriately corrected for the scattering center mass. For inverse photoemission, we used the momentum of the incident electron, probing the unoccupied band closest to E_F (9.5–11.5 eV electron kinetic energy). For all surface studies, the surface of the NiMnSb(100) epitaxial thin films[17] of 1000 Å thickness were carefully prepared by gentle Ar-sputtering and annealing treatments, as described in Ref. 2.

Figure 1 shows the temperature dependence of the intensities of the backscattered low electron diffraction spots, after background subtraction (I_{bk}) and normalization to the value (I_0) at the lowest temperature. The three sets of data shown were taken using different incident electron energies of 33, 58, and 83 eV. The angle θ from Eq. (2) varied very little in our experiment and the change in scattering vector (Δk) largely comes from the different electron energies employed.

The change in LEED intensities, shown in Fig. 1 as the slopes of $\ln[(I - I_{bk})/I_0]$, increase with increasing (Δk) or with increasing incident (and backscattered) electron ener-
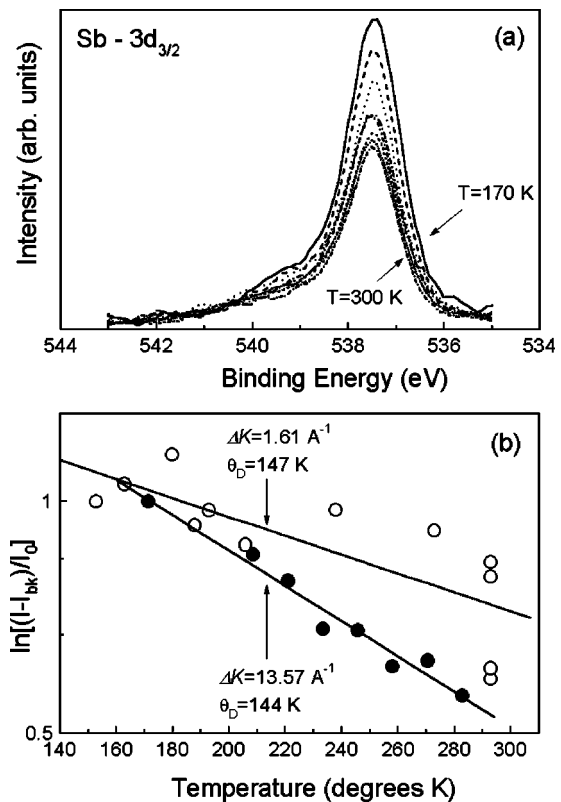

FIG. 2. (a) Normal x-ray photoemission spectra of Sb–$3d_{3/2}$ core level for various temperatures after background subtraction. The light was incident at 60° with a photon energy of 1254 eV. (b) Logarithm of the intensity of the Sb–$3d_{3/2}$ core level vs temperature (●) and the intensity of the state at the conduction band edge (just above E_F) in inverse photoemission (○).

gies. Using Eq. (1), the values obtained for the effective surface Debye temperature are 140 ± 20 K (at 33 eV incident electron energy), 143 ± 20 K (at 58 eV), and 154 ± 20 K (at 83 eV). The electron mean free path increases and so does the probing depth with increasing incident (and backscattered) electron energies. We consider the effective Debye temperature obtained at the lowest electron energies as the most representative of the dynamic normal atomic motions in the thin film surface region. The other two values, at higher electron energies, include the normal vibrations of the atoms situated increasingly deeper in the selvedge (near surface) region.

Temperature dependence of the $3d_{3/2}$ core level of antimony obtained in x-ray photoemission is shown in Fig. 2. This particular core level has a narrow and intense line shape. From Eq. (4) results a value of 144 ± 10 K for the effective surface Debye temperature. The mean free path of the ejected electrons in normal emission is no more than 20 Å from the free surface and so, the sample probing depth is limited to the surface and selvedge region. Inverse photoemission is also very surface sensitive. The intensity of the largely spin majority unoccupied band (near E_F where the electron phonon coupling is greatest),[2] in inverse photoemission, provides a value for the effective Debye temperature of about 147 ± 30 K. The value of the effective Debye temperature obtained in XPS and inverse photoemission are both representative of the harmonic vibrations of the atoms in the surface region along the film normal.

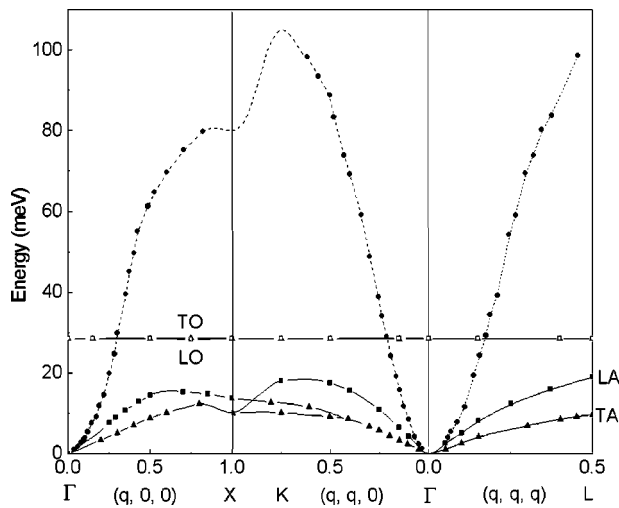For comparison, we have compared the above values

FIG. 3. Dispersion curves for magnons (●), longitudinal phonons (■), and transversal phonons (▲) at 300 K. No magnetic field was applied.

with that of bulk single crystals obtained from neutron scattering (a bulk sensitive technique). Inelastic neutron scattering experiments[19] were carried out at the Institute Laue-Langevin, using IN1 (hot neutrons) and IN8 (thermal neutrons) spectrometers, in order to cover all the values for the transfer energies from 0 to 120 meV. Excitations were investigated mainly at room temperature in the direction of the high symmetry axis (100), (110), and (111). No magnetic field was applied. Constant energy scans were generally performed to investigate the steep magnon dispersion, whereas constant-q scans were used to locate the acoustic and optical phonons. Figure 3 presents the complete experimental phonons and magnons dispersion curves at 300 K.[18] For a material with three atoms in the primitive cell, we generally expect three acoustic and six optical branches, whereas only one (two fold degenerated) branch of magnons was observed. Longitudinal acoustic phonons reach a maximum energy for q close to (0.6, 0, 0) in the $\langle 100 \rangle$ direction and (0.7, 0.7, 0) in the $\langle 110 \rangle$ direction. One very flat optical branch was observed at an energy of about 29 meV, with little difference in energy for longitudinal and transverse directions. (One explanation for this dispersionless optical mode is the arrangement of the Ni atoms in the cubic structure. Among the closest neighbor lattice sites to nickel are the vacancy sites.)

The elastic constants can be easily extracted from the slope of the acoustic modes in each Γ point, depending on the scanning direction. For the $\langle 100 \rangle$ longitudinal mode, $C_{11} = 138$ GPa, for the $\langle 110 \rangle$ transversal mode 1, $C_{44} = 45$ GPa and for the $\langle 110 \rangle$ transversal mode 2, $C_{12} = 48$ GPa.[18] Using these values to calculate the longitudinal and transversal mode velocities in Eq. (2), we obtain a value of the bulk Debye temperature of 312 ± 5 K.

Almost independent of surface orientation we would expect that the effective surface Debye temperature is of the order of 70% (i.e., $\frac{1}{\sqrt{2}}$) of the bulk value of the Debye temperature.[13–15] This is due to the fact that the surface atoms have only half of the number of nearest neighbors that surround the bulk atoms.[14] Comparing the values of the Debye temperature obtained for the NiMnSb(100) Heusler alloy, the surface temperature is almost 45% of the bulk value.

This drop in the Debye temperature between the surface and the bulk is not unexpected if we consider that the surface and selvedge region has a different composition than the bulk, under our preparation conditions.[2,4] Indeed, as shown in Ref. 4, manganese segregation occurs at the NiMnSb(100) surface.[4] In addition, there are several other phenomena that may contribute to the lowering of the surface Debye temperature with respect to the bulk. The motion of the surface atoms is not isotropic, the force constants at the surface can be appreciably different than in the bulk and, in general, the surface may contain anharmonic phonon modes that differ from the bulk.[20,21]

In conclusion, we have found the effective surface Debye temperature for the NiMnSb(100) thin film to be 145 ± 13 K, far smaller than the bulk Debye temperature of 312 ± 5 K. The reduced surface Debye temperature will lower the barriers to surface segregation and can be a consequence of the compositional difference due to segregation.

[1] C. Hordequin, J. P. Nozières, and J. Pierre, J. Magn. Magn. Mater. **183**, 225 (1998); C. T. Tanaka, J. Novak, and J. S. Moodera, J. Appl. Phys. **81**, 5515 (1997); C. T. Tanaka, J. Novak, and J. S. Moodera, J. Appl. Phys. **86**, 6239 (1999).

[2] Delia Ristoiu, J. P. Nozières, C. N. Borca, T. Komesu, H-K. Jeong, and P. A. Dowben, Europhys. Lett. **49**, 624 (2000).

[3] D. Orgassa, H. Fujiwara, T. C. Schulthess, and W. H. Butler, Phys. Rev. B **60**, 13237 (1999).

[4] D. Ristoiu, J. P. Nozières, C. N. Borca, B. Borca, and P. A. Dowben, Appl. Phys. Lett. **76**, 2349 (2000).

[5] S. C. Wang and G. Ehrlich, Surf. Sci. **206**, 457 (1988); H. Roux, A. Piquet, R. Uzun, and M. Drechsler, Surf. Sci. **59**, 97 (1976).

[6] A. D. Badorf and E. W. Plummer, J. Electron Spectrosc. Relat. Phenom. **54/55**, 541 (1990); Phys. Rev. Lett. **66**, 2770 (1991); G. Benedek and J. P. Toennies, Phys. Rev. B **46**, 13643 (1992).

[7] R. T. Tung, W. R. Graham, and A. J. Melmed, Surf. Sci. **115**, 576 (1982); D. A. King and G. Thomas, Surf. Sci. **91**, 201 (1980).

[8] C. N. Borca, J. Choi, S. Adenwalla, S. Ducharme, P. A. Dowben, L. Robertson, V. M. Fridkin, S. P. Palto, and N. Petukhova, Appl. Phys. Lett. **74**, 347 (1999).

[9] J. Zhang and E. W. Plummer, Surf. Sci. **393**, 64 (1997).

[10] E. S. R. Gopal, in *Specific Heats at Low Temperatures* (Plenum, New York, 1966), p. 29.

[11] Charles Kittel, in *Introduction to Solid State Physics* (Wiley, New York, 1996), p. 90.

[12] E. A. Soares, V. E. deCarvalho, and V. B. Nascimento, Surf. Sci. **431**, 74 (1999); S. Mroz and A. Mroz, Surf. Sci. **109**, 444 (1981).

[13] M. A. Van Hove, W. H. Weinberg, and C.-M. Chan, in *Low-Energy Electron Diffraction* (Springer Series in Surface Science, New York, 1986), Vol. 6, pp. 134.

[14] L. J. Clarke, *Surface Crystallography* (Wiley, New York, 1985).

[15] C. Waldfried, D. N. McIlroy, J. Zhang, P. A. Dowben, G. A. Katrich, and E. W. Plummer, Surf. Sci. **363**, 296 (1996).

[16] J. Choi, P. A. Dowben, S. Pebley, A. V. Bune, S. Ducharme, V. M. Fridkin, S. P. Palto, and N. Petukhova, Phys. Rev. Lett. **80**, 1328 (1998).

[17] D. Ristoiu, J. P. Nozières, and L. Ranno, J. Magn. Magn. Mater. (in press).

[18] C. Hordequin, Ph.D. thesis (unpublished).

[19] C. Hordequin, J. Pierre, and R. Currat, J. Magn. Magn. Mater. **162**, 75 (1996).

[20] L. Yang and T. S. Rahman, Phys. Rev. Lett. **67**, 2327 (1991).

[21] P. D. Ditlevsen, P. O. Stoltze, and J. K. Nørskov, Phys. Rev. B **44**, 13002 (1991).